Angewandte Chemie
Eine Zeitschrift der Gesellschaft Deutscher Chemiker

Supporting Information

Monitoring ROS Responsive Fe_3O_4-based Nanoparticle Mediated Ferroptosis&Immunotherapy via ^{129}Xe MRI

L. Zhang, M. Qiu, R. Wang, S. Li, X. Liu, Q. Xu, L. Xiao, Z.-X. Jiang, X. Zhou, S. Chen**

Supplementary Information

Monitoring ROS Responsive Fe_3O_4-based Nanoparticle Mediated Ferroptosis&Immunotherapy via ^{129}Xe MRI

Lei Zhang[a,b+], *Maosong Qiu*[a,b+], *Ruifang Wang*[a,b], *Sha Li*[a,b], *Xiaoxun Liu*[a,b], *Qiuyi Xu*[a,b], *Long Xiao*[a,b], *Zhong-Xing Jiang*[a,b], *Xin Zhou*[a,b,c], *Shizhen Chen*[a,b,c*]

[a] State Key Laboratory of Magnetic Resonance and Atomic and Molecular Physics, National Center for Magnetic Resonance in Wuhan, Wuhan Institute of Physics and Mathematics, Innovation Academy for Precision Measurement Science and Technology, Chinese Academy of Sciences-Wuhan National Laboratory for Optoelectronics, Wuhan 430071, P. R. China.

[b] University of Chinese Academy of Sciences, Beijing 100049, P. R. China.

[c] School of Biomedical Engineering, Hainan University, Haikou, Hainan 570228, China.

***** Corresponding author: chenshizhen@wipm.ac.cn

[+] These authors contributed equally to this work

Table of Contents

Materials

Unless otherwise noted, all chemicals were used without further purification. $FeCl_2 \cdot 4H_2O$, fluorescein isothiocyanate isomer (FITC), glucose oxidase (GOx), 1,2-dioctadecanoyl-sn-glycero-3-phophocholine (DSPC), 1,2-distearoyl-sn-glycero-3-phosphoethanolamine-PEG_{2000} (DSPE-PEG2000), 5,5-dimethyl-1-pyrroline N-oxide (DMPO), and IL-4 were ordered from Sigma-Aldrich (MO, USA). 3,3'-(Propane-2,2-diylbis(sulfanediyl))dipropionic acid was obtained from Bide Pharmatech Ltd. (Shanghai, China). Polyvinyl pyrrolidone K30 (PVP-K30), triethylamine, N,N-dimethylformamide (DMF), ethanol (CH_3CH_2OH), dichloromethane, Na_2HPO_4, NaH_2PO_4, methylene blue (MB), glucose, and triethylamine (TEA) were purchased from Sinopharm Chemical Reagent Co., Ltd. (Shanghai, China). Tuftsin and ferroptosis inhibitor ferrostatin-1 (Fer-1) were obtained from MedChemExpress (USA). DMEM and 1640 medium were purchased from Boster Company (China). Cholesterol, 4',6-diamidino-2-phenylindole (DAPI), 2',7'-dichlorodihydrofluorescein diacetate (DCFH-DA), lipid peroxidation probe (Liperfluo) BODIPY™ 581/591 C11, and hydrogen peroxide Assay Kit were obtained from Solarbio (Beijing, China). Mitochondrial membrane potential Assay Kit with JC-1, Calcein/PI cell viability/cytotoxicity Assay Kit, and Annexin V-FITC/PI Apoptosis Kit were obtained from Beyotime Biotechnology Co. Ltd. (Shanghai, China). Anti-glutathione peroxidase 4 antibody (GPX4) was purchased from Santa Cruz Biotechnology (USA). Antibodies against CD45, CD3, CD4, CD8, CD25, FOXP3, CD11b, F4/80, CD80, CD86, CD206, CD11c, MHCII, CD44, and CD62L for flow cytometry were

purchased from Thermo Fisher (Waltham, USA). Anti-mouse α-PD-L1 was purchased from BioLegend (USA).

The preparation of FGTL nanoparticles

Firstly, the ROS-responsive Fe_3O_4 nanoparticles were prepared via the hydrothermal method[1]. In brief, the 107 μL of $FeCl_2 \cdot 4H_2O$ DMF solution (251.5 mM), 347 μL of 3,3'-(Propane-2,2-diylbis(sulfanediyl))dipropionic acid (ROS-responsive ligand) DMF solution (59.4 mM), 300 mg of PVP-K30, and 50 μL of TEA were well-mixed. Next, 13 mL of DMF/ethanol (1:1) mixed solution was added. After that, the mixture was transferred to a reaction kettle, where it was heated to 150 °C and reacted for 24 h. Finally, the ROS-responsive Fe_3O_4 nanoparticles were obtained via centrifugation (10000 rpm, 10 min) and washed three times with ethanol.

Subsequently, GOx and immune-activating peptides Tuftsin were loaded into ROS-responsive Fe_3O_4 nanoparticles. In detail, 10 mg of Fe_3O_4 nanoparticles were mixed with 2 mg GOx and 1 mg Tuftsin. After stirring for 24 h at 4 °C in the dark, the products were acquired through centrifugation (10000 rpm, 10 min) and washed with PBS three times. Finally, the ROS-responsive Fe_3O_4 nanoparticles loaded with GOx and Tuftsin (Fe_3O_4@GOx@Tuftsin, denoted as FGT) were obtained and redispersed in the PBS at 4 °C for further use.

At last, the FGT nanoparticles were further decorated with lipids[2]. Briefly, the DSPC (65 mg), DSPE-PEG (10 mg), and cholesterol (25 mg) were dissolved in dichloromethane and ultrasound at 4 °C. Afterward, lyophilized FGT nanoparticles

(25 mg) were added into the above solution and mixed well. After spin-drying on a rotary evaporator at 40 °C, the PBS was added, and ultrasound at 4 °C to acquire FGT@Lipids (FGTL) nanoparticles. To remove free lipids, the prepared FGTL nanoparticles were purified via gel column chromatography by washing with PBS, and the purified FGTL nanoparticles were obtained. Additionally, IR820 or FITC were chosen to load into FGTL (denoted as FGITL or FGFTL) for *in vivo* fluorescence imaging and cellular uptake experiments, respectively.

Characterization of the nanoparticles

The morphology structures of Fe_3O_4 and FGTL were observed by the TEM (FEI Company, USA). The elements distribution of FGTL was shown by the HAADF-STEM (Oxford x-met 8000). Dynamic light scattering (DLS) and zeta potential measurements were carried out with a ZS nanohybrid analyzer (Malvern, England). Ultraviolet-visible-near infrared (UV–vis–NIR) absorption spectrum of various samples was measured through an Evolution 220 UV–vis spectrophotometer (Thermo Fisher Scientific Inc., USA). The values of Fe in various valence states were determined using XPS (ESCA Lab 250, Thermo Fisher Scientific, USA) experiments. Agilent 5110 Series inductively coupled plasma atomic emission spectrometry (ICP-AES, USA) was used to determine Fe element concentration. The crystalline structures of ROS-responsive Fe_3O_4 nanoparticles with or without were measured by X-ray diffraction (XRD) analysis on a D8 Focus diffractometer (Bruker, Germany). The pore diameter distribution of ROS-responsive Fe_3O_4 was obtained on the nitrogen

adsorption apparatus (ASAP 2420, Micromeritics, USA). Magnetic studies were measured by a Lakeshore 7404 high-sensitivity vibrating sample magnetometer (VSM) with fields of up to five teslas at room temperature. The ^{1}H MRI experiments were carried out on a 9.4 T micro-imaging system (Bruker Avance 400, Ettlingen, Germany).

·OH production by the POD-like activity of FGTL

In detail, the FGTL (100 μg mL^{-1}) and MB (20 μg mL^{-1}) were mixed in PB buffer at different pH with or without H_2O_2 (1 mM), glucose (1 mg mL^{-1}), or GSH (10 mM) and stood at 37 °C for 2 h. Besides, the FGTL (100 μg mL^{-1}), H_2O_2 (1 mM), and MB (20 μg mL^{-1}) were well-mixed and allowed to react at 37 °C at various times. Subsequently, the ·OH-induced MB degradation was evaluated by the observation of change in UV-vis-NIR absorbance at 665 nm.[3] The electron spin resonance (ESR) technology was used to confirm the generation of ·OH and the DMPO was chosen as the trapping agent.

GOx and Tuftsin release behavior

FGL (5 mg) or FTL (5 mg) was first dispersed in the PB buffer and treated with various concentrations of H_2O_2 or glucose, followed by transfer to the dialysis bags (300 kDa). Then, the dialysis bags were cultured in different conditions under stirring (200 rpm) at 37 °C. The 1 mL of medium was removed at the incubation times of 0.5, 1, 2, 4, 8, and 12 h, respectively, subsequent 1 mL of fresh medium was added to the culture medium. Finally, the release of GOx (276 nm) and Tuftsin (208 nm) was

measured via UV-vis spectroscopy.

Enzyme activity stability testing of GOx loaded in FGTL

To evaluate the stable activity of GOx loaded in the FGTL, the FGTL stored at 4 °C for different days was mixed with glucose (1 mg/mL). After the reaction at 37 °C for 4 h, the generation of H_2O_2 was determined by the hydrogen peroxide Assay Kit. The production of H_2O_2 represents the enzyme activity of GOx loaded in the FGTL, and the enzyme activity of GOx on day 0 was regarded as 100%.

***In vitro* ^{1}H MRI of FGTL**

The ^{1}H T_1-weighted and T_2-weighted MRI of the FGTL solution was performed on the 9.4 T micro-imaging system (Bruker Avance 400, Ettlingen, Germany). Various concentrations of FGTL based on Fe (C_{Fe} = 0.012, 0.025, 0.05, 0.1 0.2 mM) were dispersed into PBS with or without 1 mM H_2O_2, respectively. After reacting for 4 h, the ^{1}H T_1-weighted and T_2-weighted MRI of different samples were performed based on a RARE sequence. The parameters of ^{1}H T_1-weighted MRI are as follows: TR = 500 ms, TE = 11 ms, FOV = 3.5 cm × 3.5 cm, 1 mm slice thickness, RARE factor = 4, matrix size = 256 × 256, number of average = 10. The parameters of ^{1}H T_2-weighted MRI are as follows: TR = 2500 ms, TE = 36 ms, FOV = 3.5 cm × 3.5 cm, 1 mm slice thickness, RARE factor = 4, matrix size = 256 × 256, number of average = 10.

Cell culture

4T1, A549, B16F10, LLC, and RAW264.7 cell lines were obtained from the cell bank

of the Chinese Academy of Sciences (Shanghai, China) and cultured with the basic medium containing 10% FBS, 100 U mL^{-1} penicillin, and 100 U mL^{-1} streptomycin in a humidified 5% CO_2 incubator at 37 °C. All reagents were ordered from Boster Company (Wuhan, China) and were filtered through a 0.2 μm sterile filter before cell incubation.

In vitro cell uptake of FGFTL

The LLC cells were incubated with FGFTL (50 μg mL^{-1}) at 37 °C for 0.5 h, 2 h, 4 h, and 6 h, respectively. Then, the LLC cells were washed with PBS three times to remove the unabsorbed nanoparticles. At the end, the fluorescence images and fluorescence intensity analysis of LLC cells were performed on the confocal laser scanning fluorescence microscope (CLSM) imaging system (A1R/A1, Nikon, Japan) and flow cytometry (Beckman Coulter).

In vitro immune escape of FGFTL

The RAW264.7 macrophage cells were used to evaluate the effects of FGTL on the escape of the immune system. Firstly, the RAW264.7 cells were seeded into 6-well plates (1×10^5 cells $well^{-1}$) and cultivated for 24 h. Subsequently, the cells were cultured with FGFT or FGFTL (50 μg mL^{-1}) for 4 h. After washing with PBS three times, the LLC cells were fixed with 4% paraformaldehyde (10 min) and stained with DAPI (4 min) for the observation via CLSM or fluorescence analysis by flow cytometry.

Intracellular detection of ROS, LPO, and mitochondrial dysfunction

Typically, DCFH-DA, BODIPY™ 581/591 C11, and JC-1 were used as the probe to evaluate the ROS generation, lipid peroxidation, and mitochondrial dysfunction in the LLC cells, respectively. Specifically, the LLC cells were seeded in a culture dish at a density of 1×10^5 cells per dish and incubated with different samples (I: PBS, II: GOx, III: Fe_3O_4, IV: FGTL, and V: FGTL plus Fer-1) for 8 h. Then, the LLC cells were washed with PBS three times and stained by DCFH-DA for 60 min, BODIPY™ 581/591 C11 for 30 min, and JC-1 for 20 min, respectively. After that, CLSM images were carried out to evaluate the ROS generation, lipid peroxidation, and mitochondrial dysfunction in the LLC cells. Moreover, the LLC cells in groups I and IV were further characterized by TEM imaging for the observation of mitochondrial dysfunction.

Western-blot analysis

For western blots of GPX4 expressions, the LLC cells were seeded on the 6-well plates (1×10^5 cells per well) and suffered from different treatments (I: PBS, II: GOx, III: Fe_3O_4, IV: FGTL, and V: FGTL plus Fer-1) for 12 h. subsequently, the LLC cells were washed with PBS three times and lysed by the RIPA lysis buffer, and the total protein was harvested by centrifugation at 4 °C (12000 rpm, 15 min). Western blotting (Gel DocTM XR +, Bio-Rad) and ImageJ software were applied to determine the protein expression of GPX4.

***In vitro* FGTL-mediated ferroptosis**

The cytotoxicity of FGTL at different concentrations against various cell lines including 4T1 cells, A549 cells, B16F10 cells, and LLC cells was determined by using the standard CCK8 assays[4] (mean ± SD, n = 6). After incubation in a 96-well plate (1×10^4 cells per well) for 24 h, the various cells were washed with PBS and then incubated with different concentrations of FGTL (0, 25, 50, 100, 200, and 400 μg mL^{-1}) for 24 h. Subsequently, the cells were washed with PBS and cultivated with CCK-8 solution for 2 h at 37 °C. Ultimately, the UV-vis absorption at 450 nm per well was measured via the microplate reader. The cells cultured with medium without FGTL were used as control.

For the CLSM imaging analysis, human lung cancer A549 cells (1×10^5) were seeded in a culture dish and incubated with different samples (I: PBS, II: GOx, III: Fe_3O_4@Tuftsin@Lipids (FTL), IV: FGTL, and V: FGTL plus Fer-1) for 8 h. Subsequently, the A549 cells were stained with Calcein AM/PI to assess living cells (green) and dead cells (red) and imaged by CLSM. Besides, the LLC cells (1×10^5) suffered from the same treatment as the A549 cells in the CLSM imaging analysis was used to determine the cellular death rate by flow cytometry after staining with Annexin V-FITC/PI for 15 min.

LLC cell-based MCSs construction and tumor penetration assay

The LLC cell-based multicellular spheroids (MCSs) were constructed by the incubation LLC cell (1×10^4 per well) for three days in a 96-well plate.[5] Next, the MCSs were followed with various treatments (I: FITC@FTL, II: FGFTL, III: FGFTL

plus 1 mM H_2O_2) for 2 h. Next, the MSCs were washed with PBS three times and subsequently imaged via the CLSM.

Animal and tumor models

Female C57BL/6 mice (5-6 weeks of age) were purchased from Beijing Vital River Laboratory Animal Technology Co., Ltd and used under protocols by Animal Care and Use Committees at the Innovation Academy for Precision Measurement Science and Technology, the Chinese Academy of Sciences. For the subcutaneous LLC tumor model, the C57BL/6 mice were subcutaneously injected with LLC cells (100 μL, 5×10^6 cells mL^{-1}) on the leg. For the lung metastatic cancer model, the C57BL/6 mice were *i.v.* injection with LLC cells (100 μL, 1×10^6 cells mL^{-1}).

Hemolysis assay

According to our previous method,[6] the purified red blood cells (RBCs) were collected and diluted to 20 mL with sterile PBS. Next, the FGTL was added to the erythrocyte suspension to a final concentration of 100, 200, 300, 600, 1200, and 2500 μg mL^{-1}. After 4 h of cultivation at 37 ºC, the hemolysis phenomenon was recorded on the 540 nm spectrophotometric absorptions. The corresponding hemolysis percentage values were calculated by the following formula:

$$\text{Hemolysis (\%)} = [(A_s - A_n)/(A_p - A_n)] \times 100\%$$

While A_s represents sample absorbance, A_n (RBCs incubated with PBS) represents negative absorbance, and A_p (RBCs incubated with deionized water) represents positive absorbance. All the experiments were repeated three times.

In vivo fluorescence imaging

The fluorescence imaging (FLI) experiments were performed on an IVIS Spectrum imaging system (Perkin Elmer). When the volume of the tumor reached about 150 mm^3, the subcutaneous LLC tumor-bearing mice (n = 3) were given *i.v.* injections FGITL nanoparticles (20 mg kg^{-1}). The FLI of mice was performed at the time points of 0, 4, 8, 12, 24, and 36 h post-injection, respectively. Besides, the mice were sacrificed, and the tumor and main organs including heart, liver, spleen, lung, and kidney were harvested for *ex vivo* imaging (Ex: 745 nm; Em: 820 nm).

In vitro and in vivo immunity activation assay

For the *in vitro* macrophage polarization assay, RAW264.7 macrophages (1×10^5) were seeded into 6-well plates and cultured for 12 h. After treatment with IL-4 (30 ng mL^{-1}) for 12 h, the M2 phenotype macrophage was obtained. Subsequently, the RAW264.7 macrophages were incubated with residues of LLC cells treated with PBS, Fe_3O_4@GOx@Lip (denoted as FGL), or FGTL in a transwell chamber system. In the end, the RAW264.7 macrophages were stained with BV421 anti-F4/80, PE anti-CD86, and APC anti-CD206 antibodies. The frequency of M1 phenotype and M2 phenotype macrophages were determined by flow cytometry (n = 3).

For the *in vivo* antitumor immunity activation, the C57BL/6 mice with subcutaneous LLC tumor (about 100 mm^3) were *i.v.* injected with PBS, Fe_3O_4@GOx@Lip (FGL), or FGTL (20 mg kg^{-1}). After seven days, the single-cell suspensions of LLC tumors in different groups were obtained by the operation of fragmentation, homogenization, and enzymatic digestion, and further labeled with commercial fluorophores antibodies.

After that, the proportions of M2 phenotype macrophages ($CD86^{-}CD206^{+}F4/80^{+}$), M1 phenotype macrophages ($CD86^{+}CD206^{-}F4/80^{+}$), mature dendritic cells ($CD80^{+}CD86^{+}$), $CD4^{+}$ T cells ($CD3^{+}CD4^{+}CD8^{-}$), $CD8^{+}$ T cells ($CD3^{+}CD4^{-}CD8^{+}$), and Tregs ($CD3^{+}CD25^{+}FOXP3^{+}$) in the tumor tissues were measured by the flow cytometry (n = 3).

The gating standards are according to various controls as follows:

Negative control: Each type of cell produces non-specific fluorescence, and the fluorescence signal obtained during flow cytometry is the result of the combination of non-specific fluorescence from the cell itself and specific fluorescence from the cell surface bound to fluorescein. Therefore, it is very important to determine the strength of non-specific fluorescence of cells that are not related to fluorescein, and a negative control needs to be established at this time. This helps to more accurately distinguish between positive signals and negative fluorescent backgrounds in the analysis

FMO (fluorescence Minus one control) control: Refers to subtracting one fluorescent antibody (usually low expression and strong background fluorescence interference), while keeping other combinations unchanged. It is a special negative control and is often used in studying the expression of important phenotypic molecules, cytokines, etc. in different cell subpopulations. For example, Foxp3 FMO, which means adding only CD4 and CD25 without Foxp3 PE, compared to adding all three dyes, the extra part is the Treg cell population.

Compensation single positive tube control: Taking CD3-APC and CD4-FITC as examples mentioned above, we need to set up PE single staining tubes and FITC

single staining tubes for compensation regulation. Generally, single staining tubes require a clear positive cell group, such as CD3 and CD4 with high expression levels and obvious positive cell groups, but for some cases where antigen expression is weak (positive cell groups are invisible), such as CD25, it is necessary to use compensation microspheres in this case.

Overall, the precision gate can be obtained with the aid of Negative control, FMO control, and Compensation single positive tube control.

In vivo immunotherapy of subcutaneous LLC tumor

The subcutaneous LLC tumor model was built by subcutaneous injection of LLC cells (5×10^6) on the right flank of C57BL/6 mice. After three days of growth (set as day 0), the C57BL/6 mice were randomly divided into five groups (n = 5) and treated as follows: (I) PBS, (II) α-PD-L1, (III) Fe_3O_4@Tuftsin@Lipids (FTL), (IV) FGTL, and (V) FGTL plus α-PD-L1 (100 μL, 20 mg kg^{-1}). The mice in groups II and V were injected with α-PD-L1 (25 μg per mouse) on days 3, 5, and 7. Tumor volumes and body weights of mice were monitored every two days. Tumor volume = length × $width^2/2$.

In vivo immunotherapy of LLC lung metastases and the ^{129}Xe MRI evaluation

The lung metastases model C57BL/6 mice were built by the *i.v.* injection of LLC cells (2×10^6). After three days of growth (set as day 4), the C57BL/6 mice were randomly divided into four groups (n = 6) and treated as follows: (I) PBS, (II) α-PD-L1, (III) Fe_3O_4@Tuftsin@Lipids (FTL), and (IV) FGTL + α-PD-L1 (100 μL, 20 mg kg^{-1}). The

mice in groups II and IV were injected with α-PD-L1 (25 μg per mouse) on days 6, 8, and 10. The lung CT imaging of mice was performed on days 14 and 21. The body weights of mice were monitored every two days until day 22. On day 22, the mice were sacrificed and the lungs were harvested for the photography and H&E staining. The spleens were obtained, homogenized, and enzymatically digested to prepare single-cell suspensions for antibody labeling. Subsequently, the frequency of central memory T cells (T_{CM}, $CD62L^+CD44^+$) and effector memory T cells (T_{EM}, $CD62L^-CD44^+$) were determined by flow cytometry (n = 3).

Another batch of lung metastases model C57BL/6 mice was followed with various treatments as above described to further evaluate the FGTL-mediated ferroptosis-enhanced immunotherapy efficacy by ^{129}Xe MRI. On day 22, the ^{129}Xe ventilation MRI and chemical shift saturation recovery (CSSR)[7] experiments of the lung in all groups were performed.

Statistical analysis

All the data are presented as mean ± standard deviation (SD). Experiments were performed in triplicate unless otherwise stated. The statistical analysis was performed using the GraphPad Prism software (version 9.0.0). Student's t-test determined the significance of the difference between the two groups (*****$p < 0.05$, ******$p < 0.01$, *******$p < 0.001$).

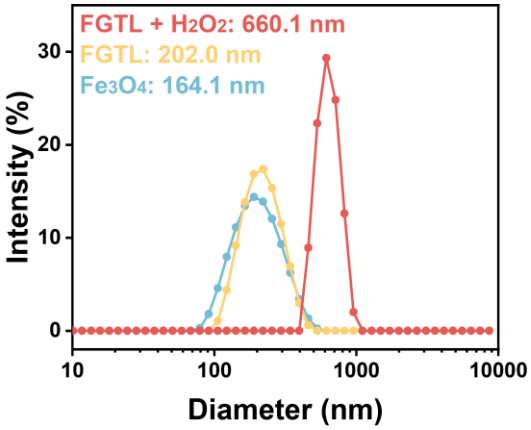

Figure S1. Hydrodynamic diameters of Fe_3O_4, FGTL, and FGTL plus 1 mM H_2O_2.

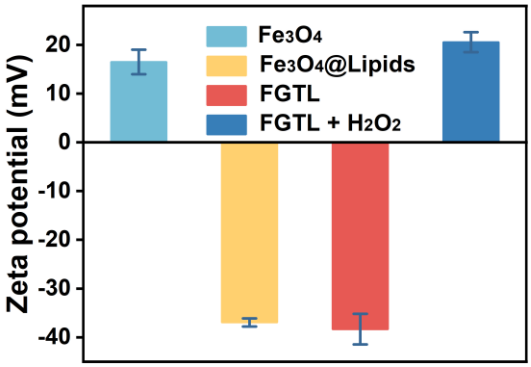

Figure S2. Zeta potentials of Fe_3O_4, Fe_3O_4@Lipids, FGTL, and FGTL + 1 mM H_2O_2.

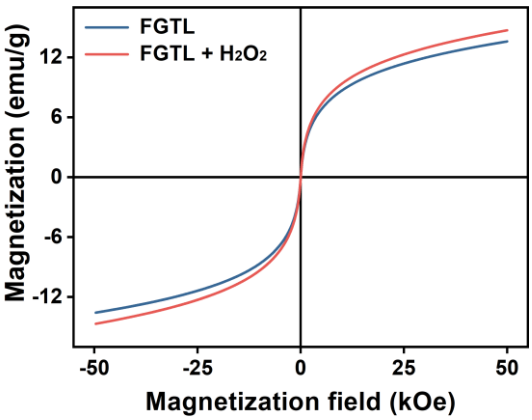

Figure S3. Magnetization curves of the FGTL with or without treatment of 1 mM H_2O_2, illustrated the superparamagnetic property of the FGTL.

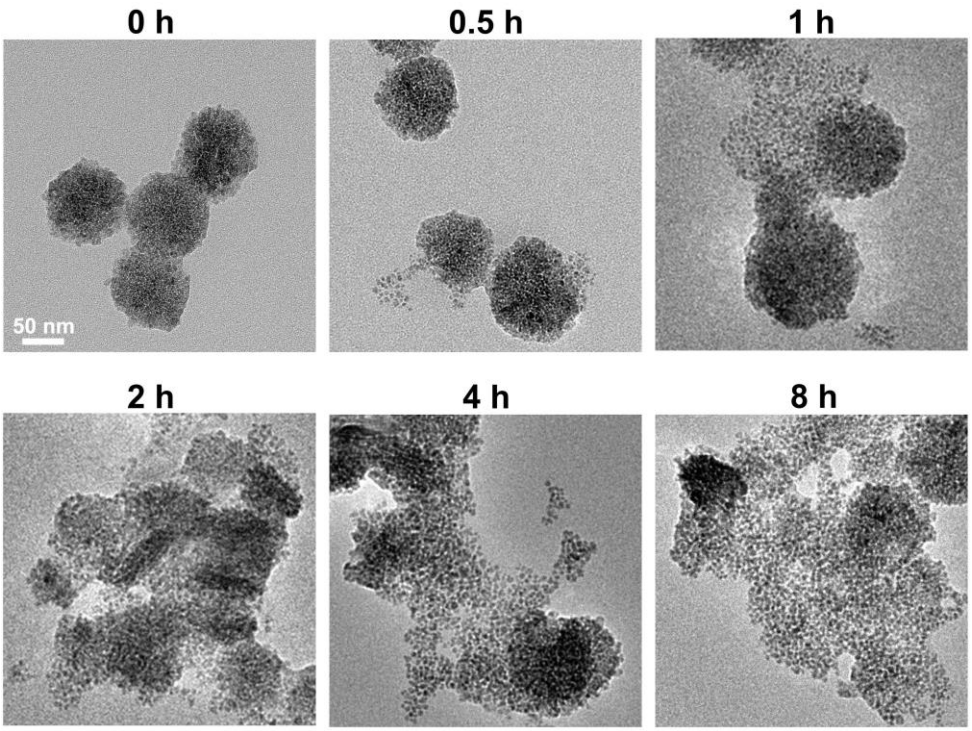

Figure S4. The TEM images of FGTL nanoparticles after incubation with 1 mM H_2O_2 for 0, 0.5, 1, 2, 4, and 8 h, respectively.

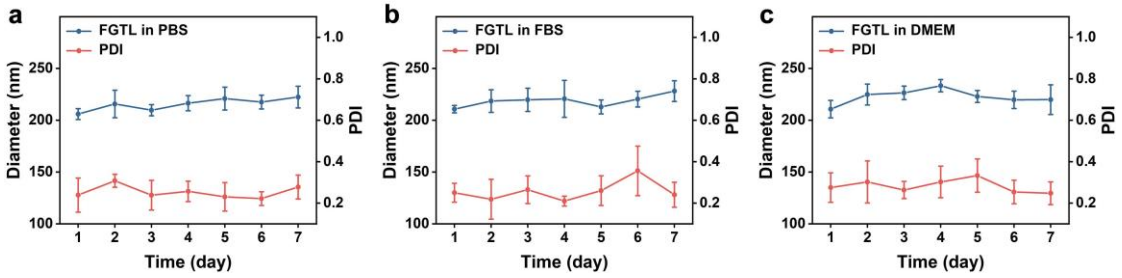

Figure S5. The stability of FGTL in PBS, 10% fetal bovine serum-containing PBS, and DMEM over seven days.

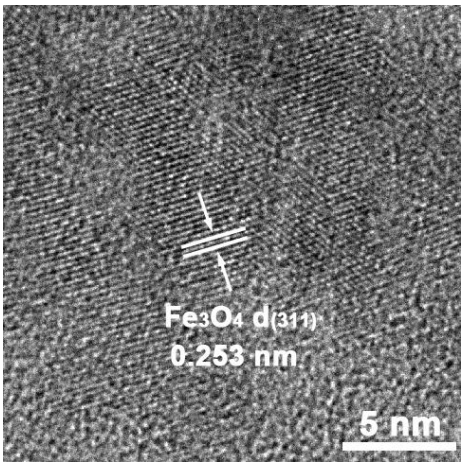

Figure S6. HRTEM images of Fe_3O_4 nanoparticles. The images clearly show the single crystallinity of the Fe_3O_4.

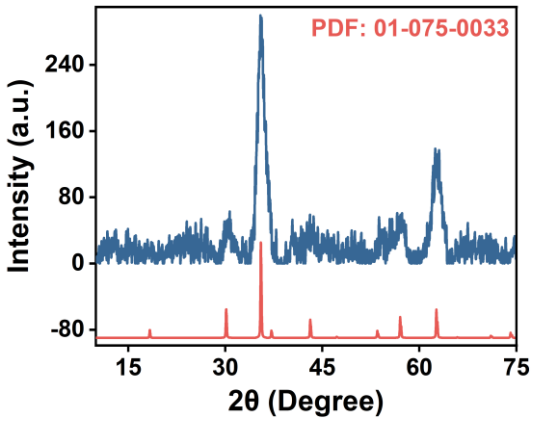

Figure S7. The XRD of ROS-responsive Fe_3O_4 nanoparticles after incubation with 1 mM H_2O_2 for 4 h.

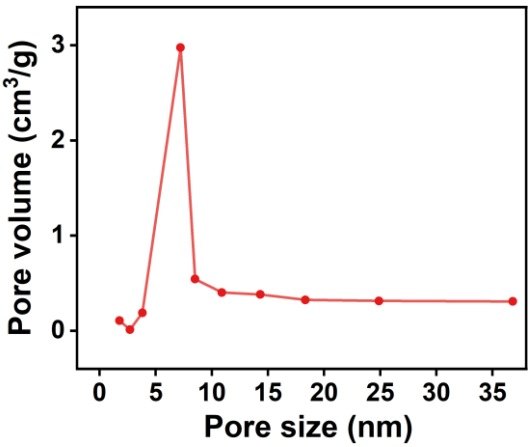

Figure S8. The pore size distribution of ROS-responsive Fe_3O_4.

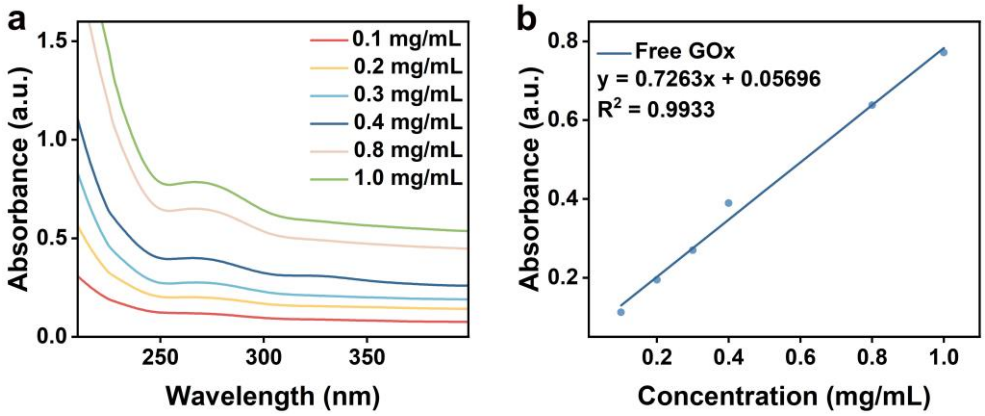

Figure S9. The UV-vis-NIR absorption spectra and corresponding standard curves of free GOx.

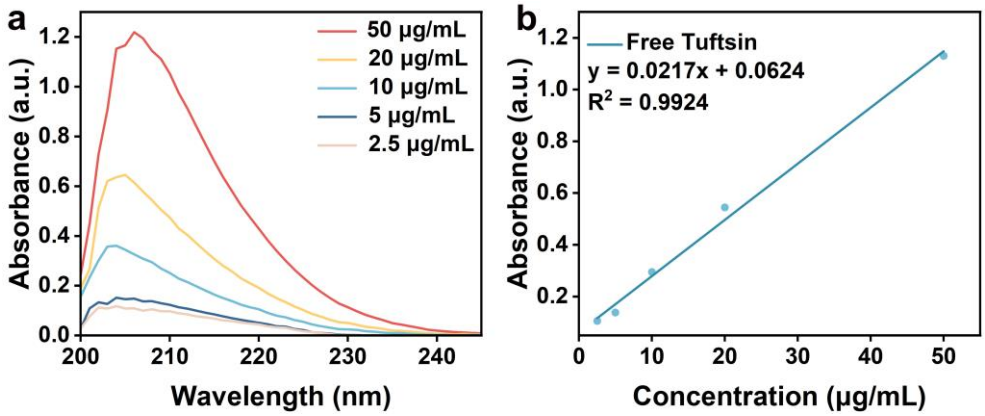

Figure S10. The UV-vis-NIR absorption spectra and corresponding standard curves of Tuftsin.

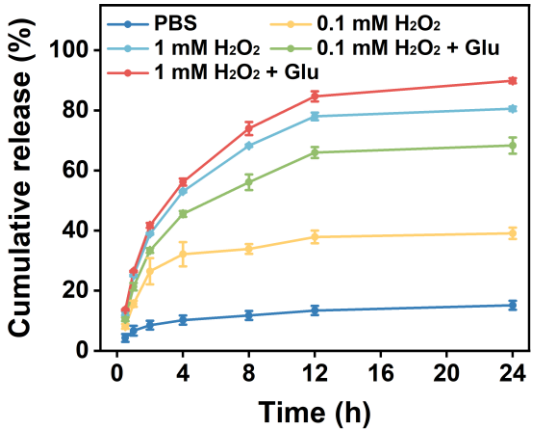

Figure S11. Cumulative release of GOx from FGL (without Tuftsin) incubated at different conditions (mean ± SD, n = 3).

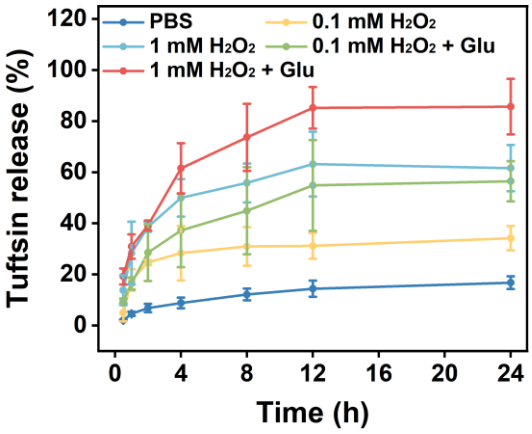

Figure S12. Cumulative release of Tuftsin from FTL (without GOx) incubated at different conditions (mean ± SD, n = 3).

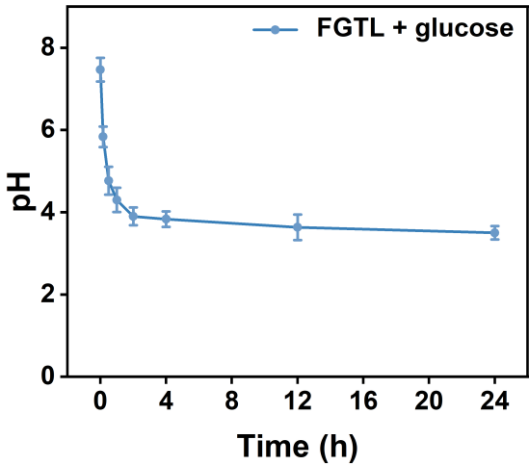

Figure S13. pH values at various time points arising from FGTL (glucose: 5 mM). The results showed that the pH values gradually decreased with the duration of the reaction, which is beneficial for the progress of the Fenton reaction.

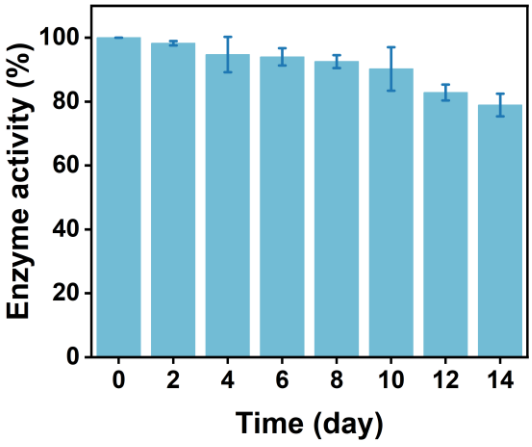

Figure S14. The activity of GOx loaded in FGTL after storage for different days.

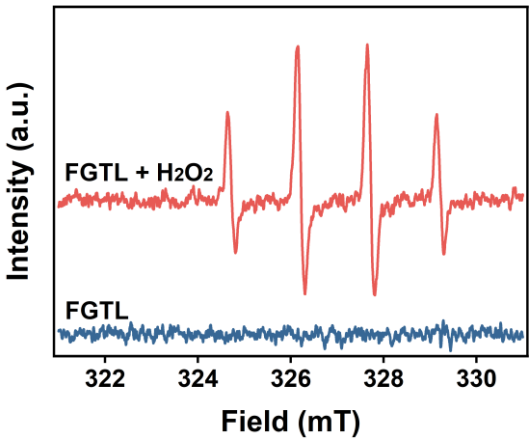

Figure S15. The ESR spectra of FGTL and FGTL plus 1 mM H_2O_2 (indicating ·OH).

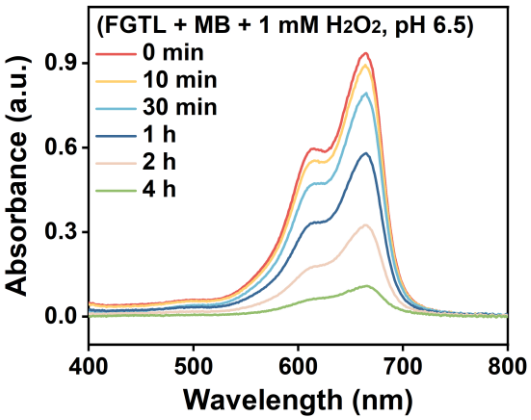

Figure S16. The UV-vis-NIR absorption spectrum of MB after incubation with FGTL plus 1 mM H_2O_2 (pH 6.5) at different times, confirmed the persistent performance of the POD-like enzyme activity of FGTL.

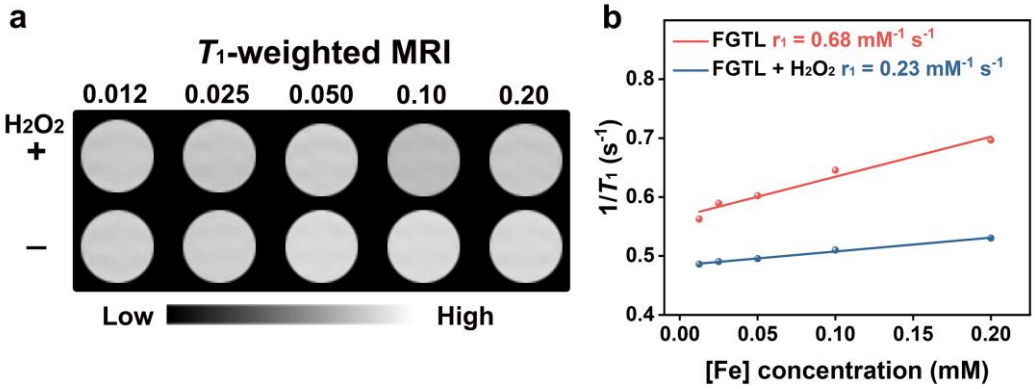

Figure S17. (a) ^1H T_1-weighted MRI of various concentrations of FGTL with or without treatment of 1 mM H_2O_2 and (b) the corresponding r_1 values.

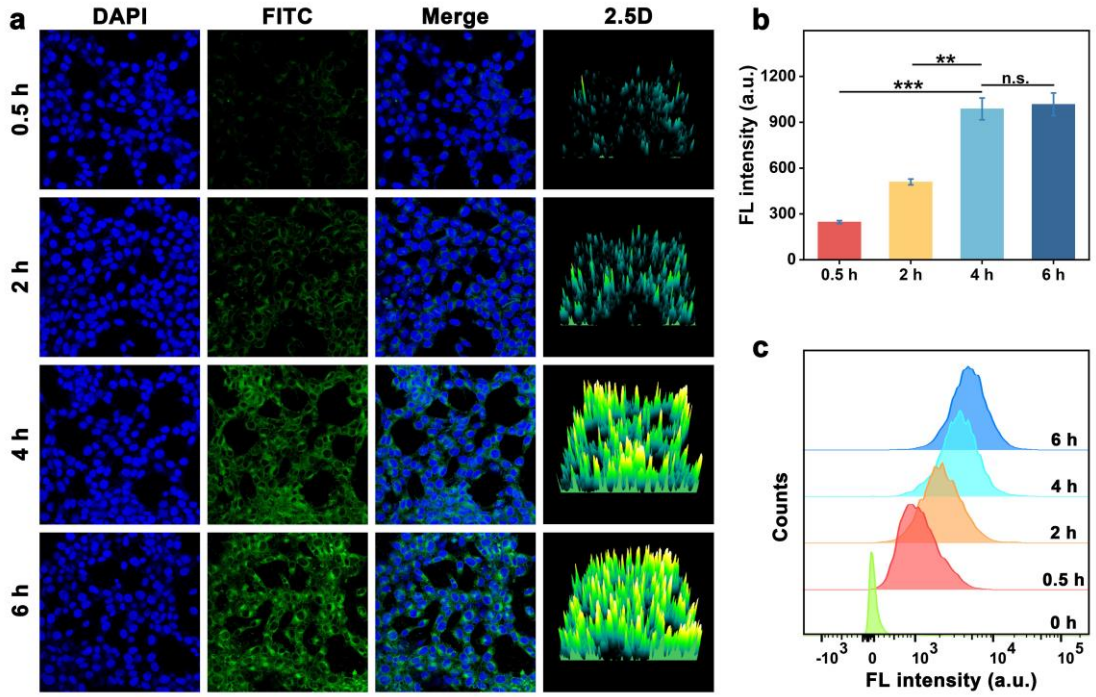

Figure S18. Intracellular uptake of FITC@FGTL. (a) CLSM images of LLC cells incubated with FGTL (50 μg·mL^{-1}) for 0.5 h, 2 h, 4 h, and 6 h, respectively, and (b) the corresponding fluorescence intensity analysis of CLSM images (mean ± SD, n = 3, n.s.: no significance, ** $p < 0.01$, *** $p < 0.001$). (c) Flow cytometry quantification of LLC cells incubated with FGTL at various times.

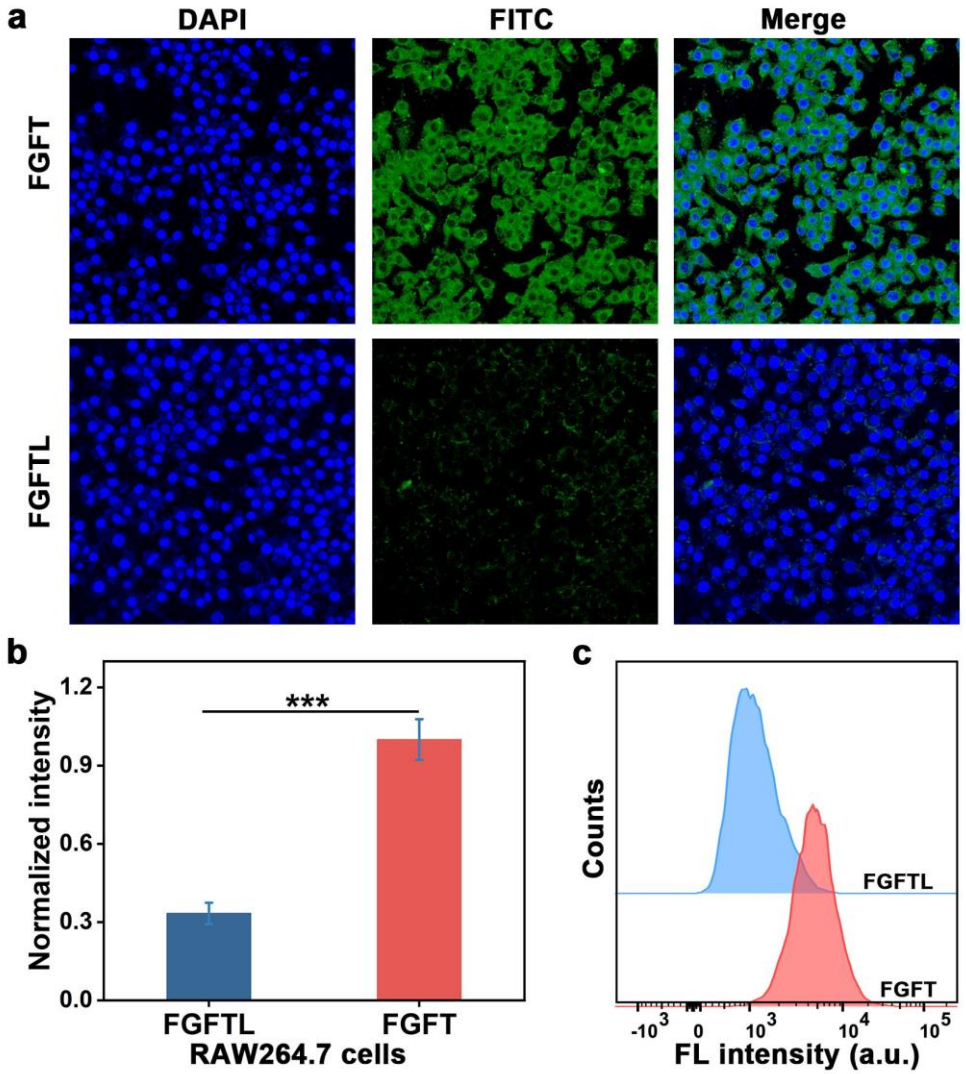

Figure S19. (a) Confocal images of RAW264.7 cells after treatment with FGFT and FGFTL (50 μg·mL^{-1}) for 4 h, respectively, and (b) the corresponding fluorescence intensity analysis of CLSM images (mean ± SD, n = 3, ***p < 0.001) and (c) flow cytometry quantification analysis.

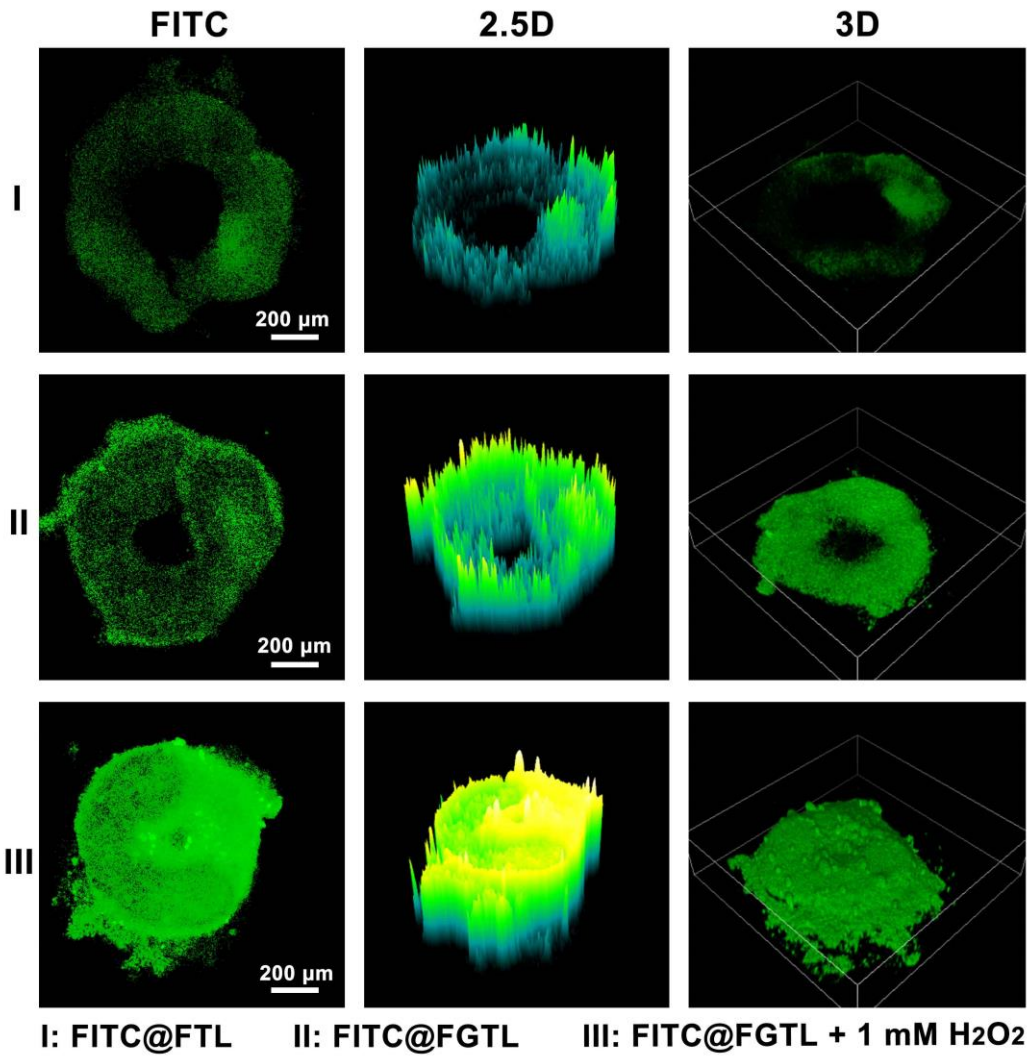

Figure S20. The tumor penetration images of LLC cell-based multicellular spheroids after incubation with FITC@FTL, FITC@FGTL, and FITC@FGTL plus 1 mM H_2O_2 for 2 h, respectively (dose: 50 μg·mL^{-1}).

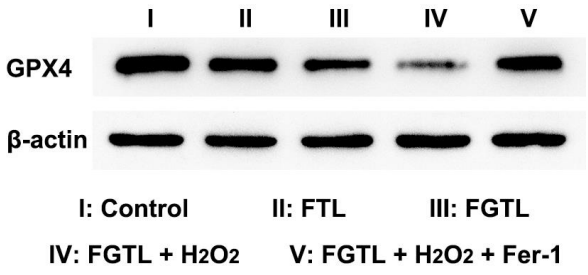

Figure S21. Western blot analysis of GPX4 expression in LLC cells after different treatments (nanoparticles concentration: 50 μg mL^{-1}).

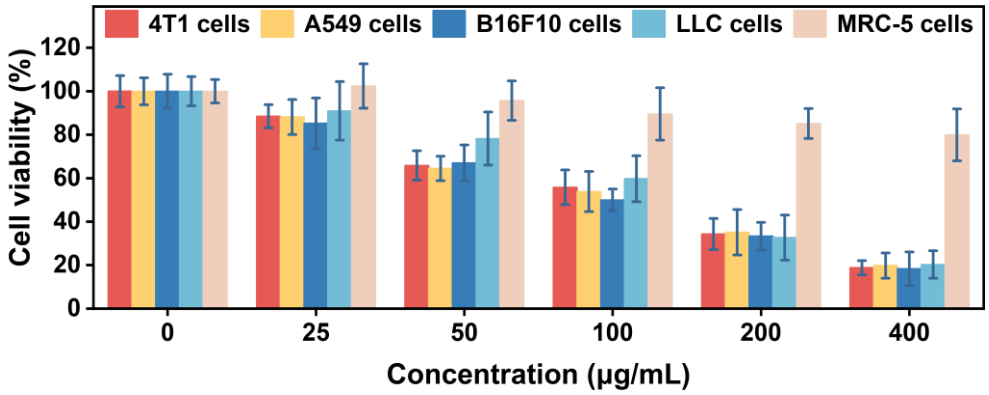

Figure S22. The cell viability of 4T1, A549, B16F10, LLC, and MRC-5 cells after treatment with FGTL at different concentrations for 24 h (mean ± SD, n = 6).

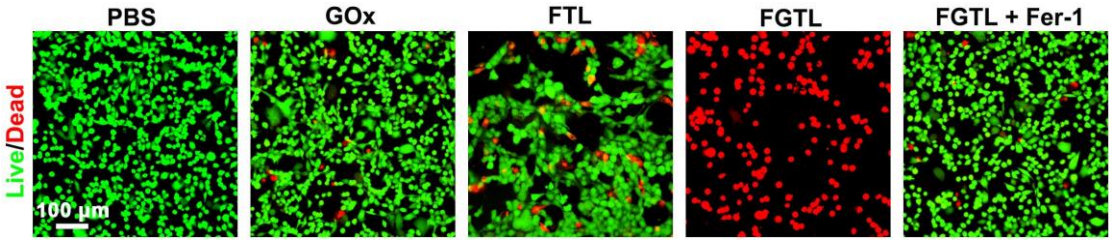

Figure S23. CLSM images of LLC cells live/dead staining with Calcein-AM/PI (green/red) after different treatments for 24 h (dose: 200 μg mL^{-1}).

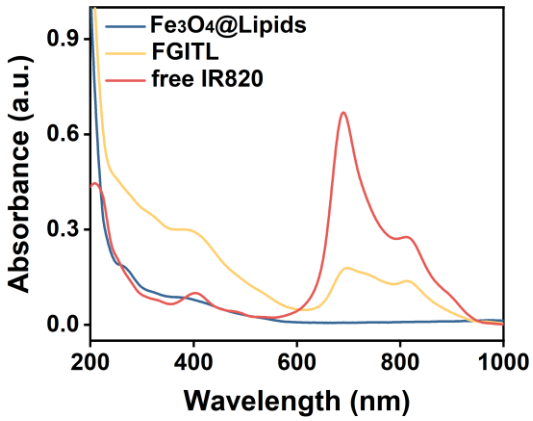

Figure S24. UV-vis-NIR absorption spectra of Fe_3O_4@Lipids, FGITL, and free IR820.

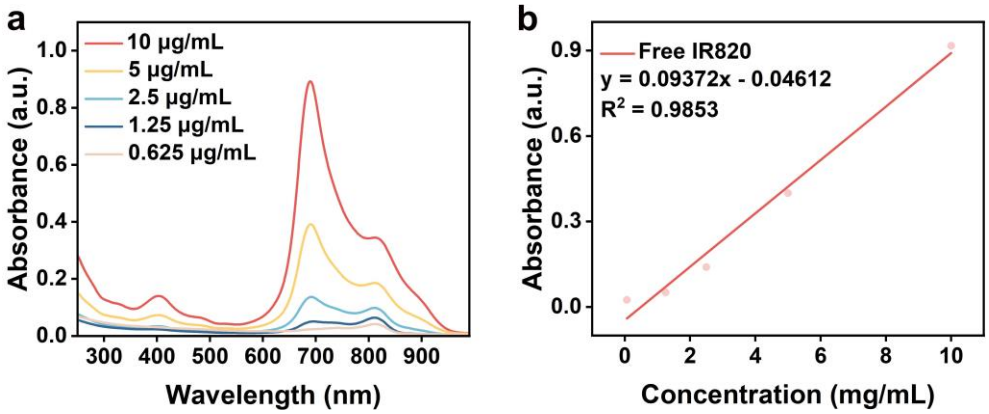

Figure S25. UV-vis-NIR absorption spectra and corresponding standard curve of IR820.

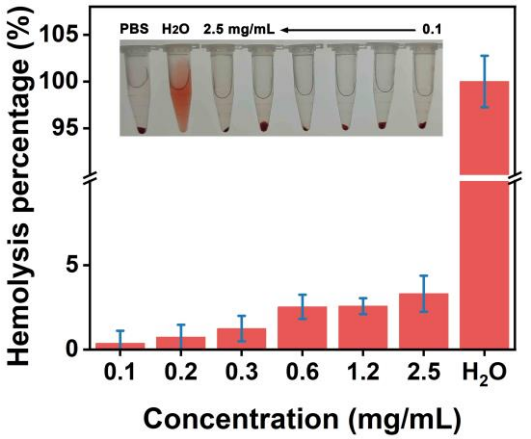

Figure S26. *In vitro* hemolysis percentage of FGTL incubated with mice RBCs at 37 °C for 4 h at various concentrations. PBS was set as the negative control and deionized water was set as the positive control (mean ± SD, n = 3). The results confirmed the qualified hemolysis rate of FGTL.

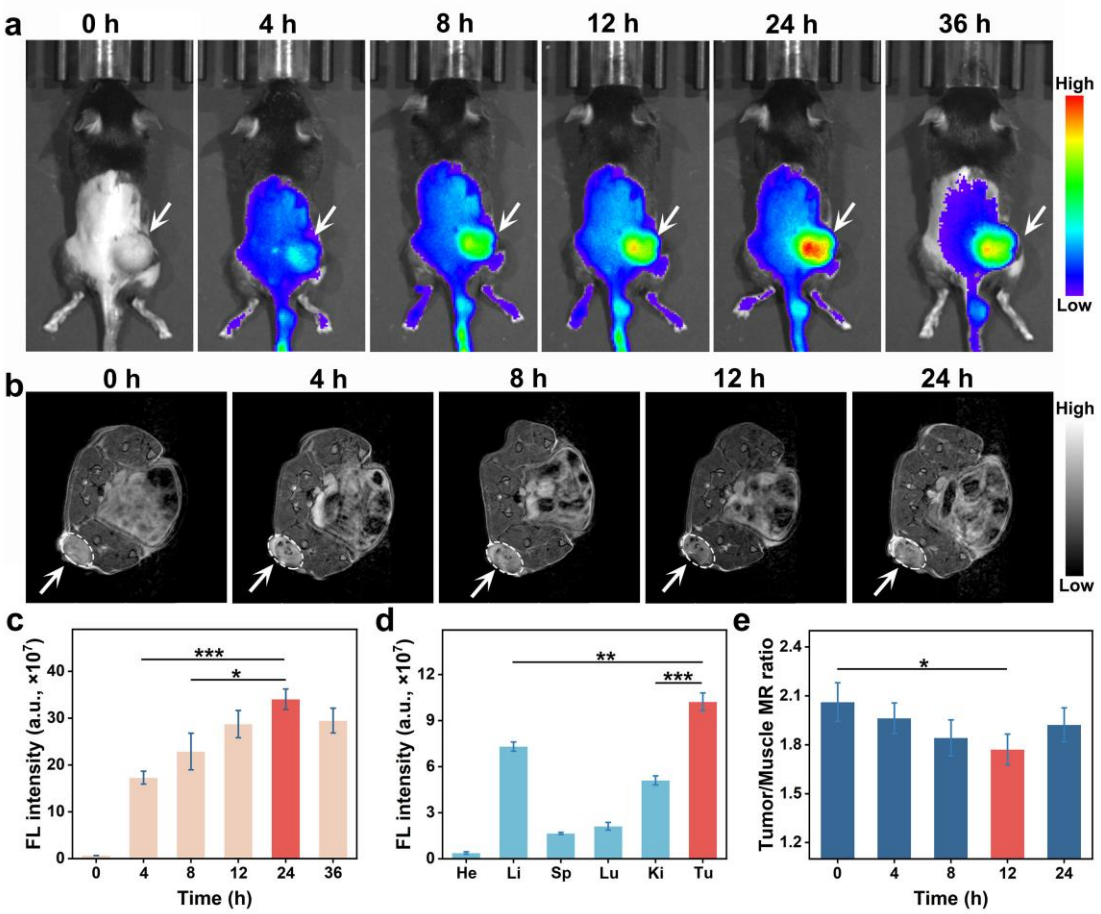

Figure S27. *In vivo* FLI/^{1}H T_2-weighted MRI of FGTL. (a) Fluorescence imaging and (b) ^{1}H T_2-weighted MRI of subcutaneous LLC tumor-bearing mice after *i.v.* injection of FGITL (arrows indicate tumors). (c) The corresponding fluorescence intensity analysis of the tumor region and (d) the isolated organs and tumor (mean ± SD, n = 3, **p* < 0.05, ***p* < 0.01, ****p* < 0.001). (e) The corresponding tumor/muscle MR ratio (mean ± SD, n = 3, **p* < 0.05).

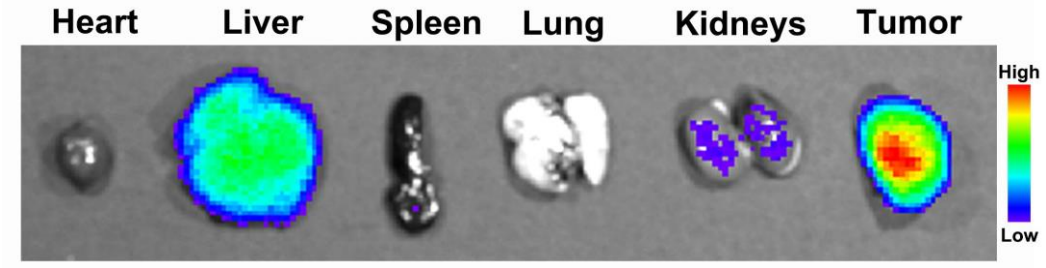

Figure S28. Fluorescence imaging of isolated organs (heart, liver, spleen, lung, and kidney) and tumor obtained from C57BL/6 mice at 36 h post-injection of FGITL.

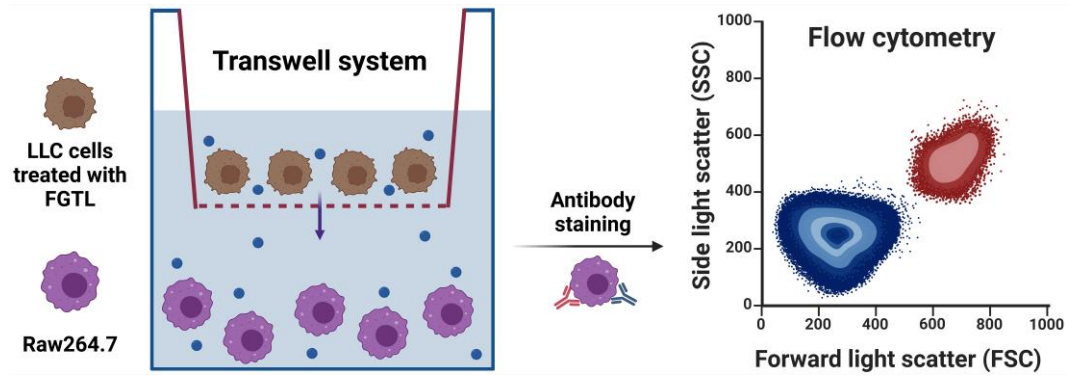

Figure S29. Schematic illustration of M2 phenotype macrophages polarized to M1 phenotype via the transwell insert system upon coincubation with LLC cells pre-treated with PBS, FGL, and FGTL, respectively.

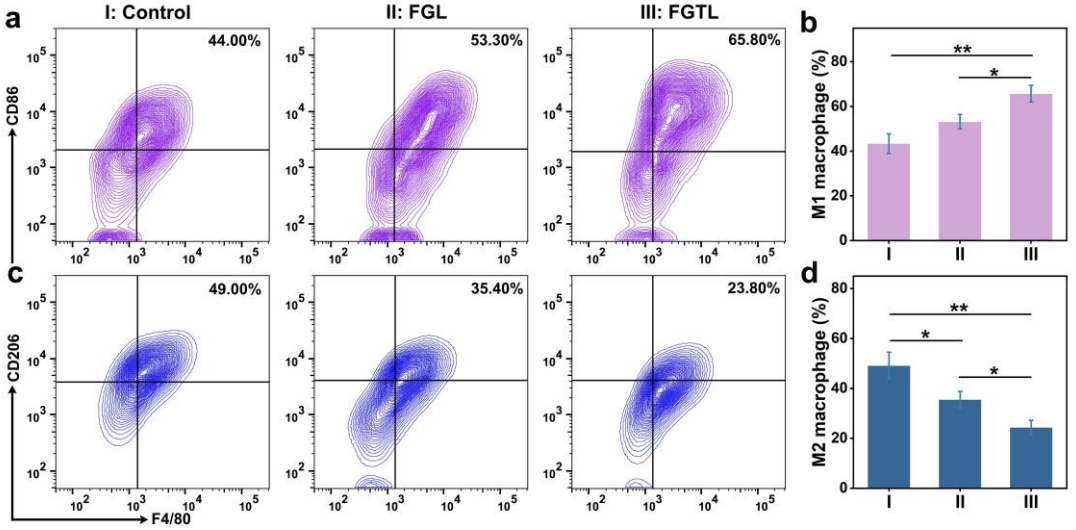

Figure S30. *In vitro* immune activated by FGTL. (a) Representative FCM and (b) the relevant quantitative analysis of M1 phenotype macrophages and M2 phenotype macrophages (mean ± SD, n = 3, ***p* < 0.05, ****p* < 0.01).

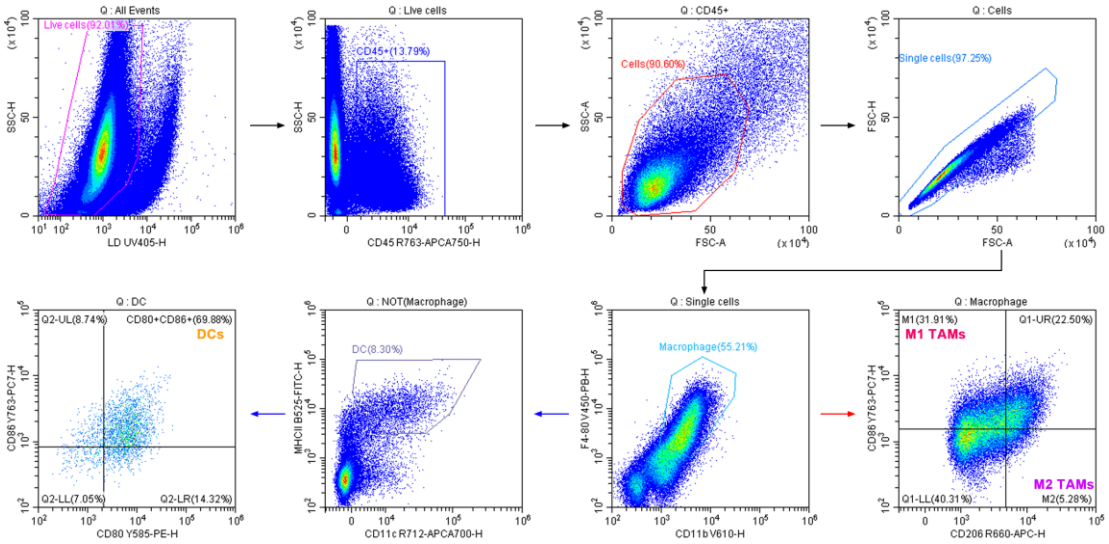

Figure S31. Representative flow cytometry gating strategies for mature dendritic cells ($CD11c^{+}MHC\ II^{+}CD80^{+}CD86^{+}$), M1 tumor-associated macrophages ($CD11b^{+}F4\text{-}80^{+}CD206^{-}CD86^{+}$), and M2 tumor-associated macrophages ($CD11b^{+}F4\text{-}80^{+}CD206^{+}CD86^{-}$).

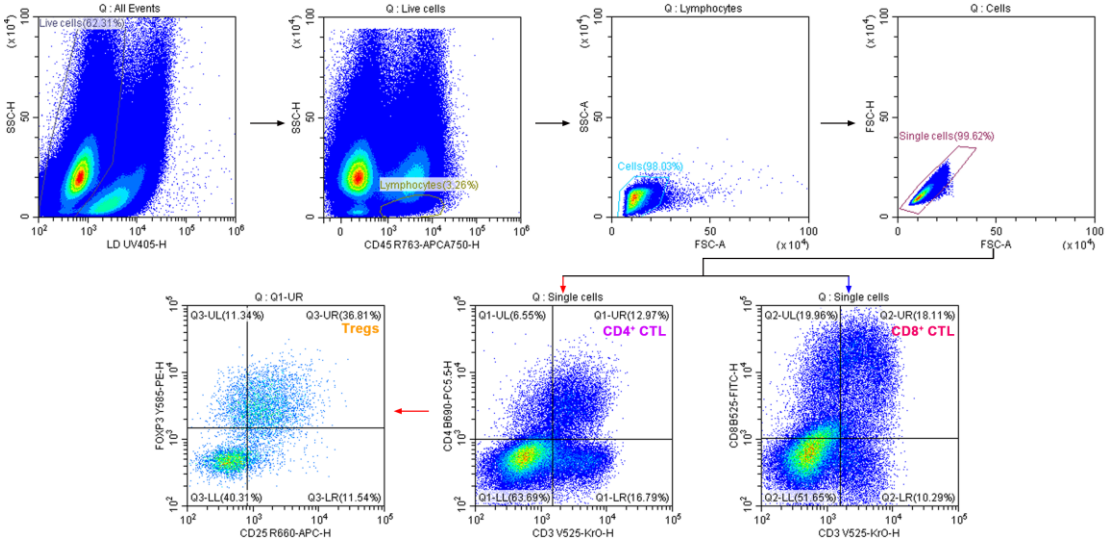

Figure S32. Representative flow cytometry gating strategies for cytotoxic T cells ($CD3^{+}CD8^{+}$), helper T cells ($CD3^{+}CD4^{+}$), and Treg ($CD4^{+}CD25^{+}FOXP3^{+}$).

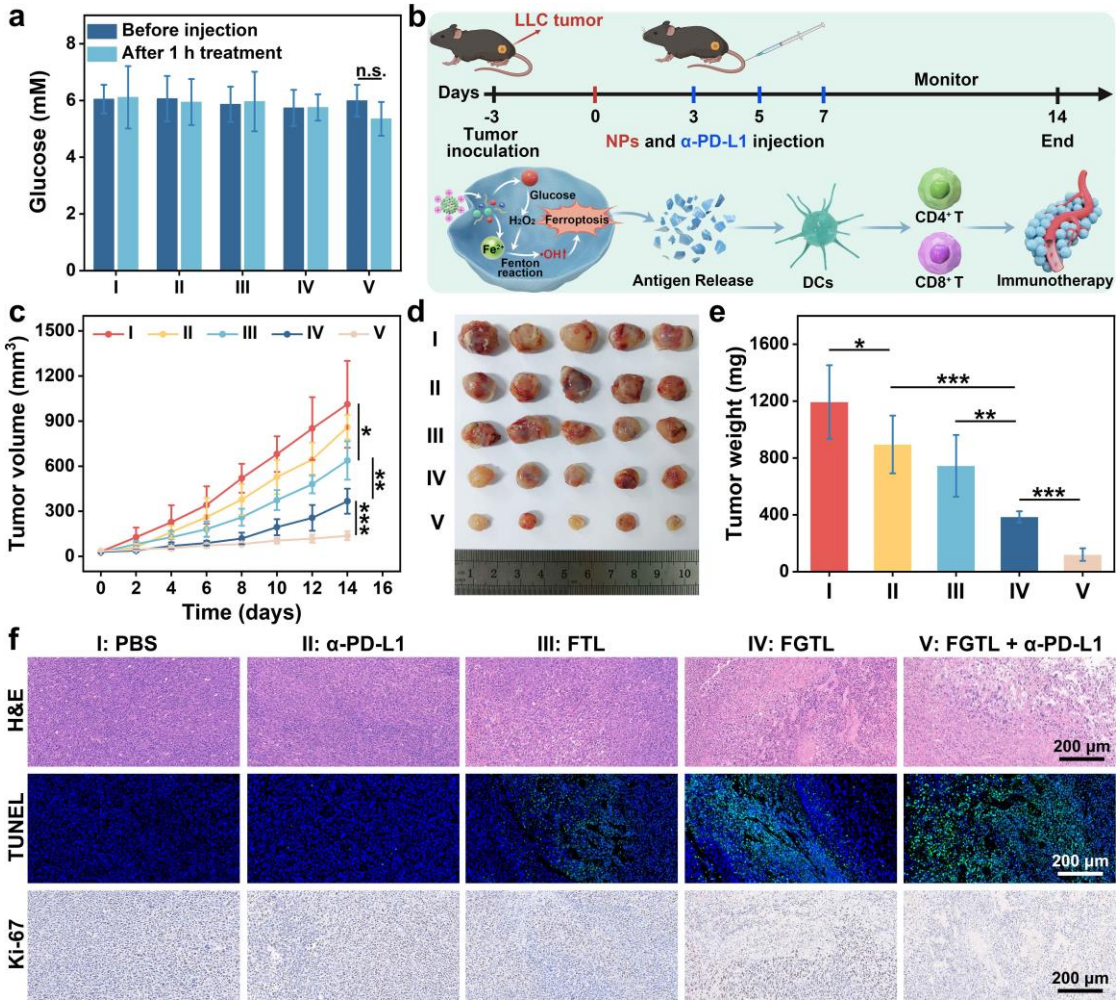

Figure S33. *In vivo* FGTL-mediated ferroptosis enhanced immunotherapy of LLC tumor-bearing mice. (a) Changes in blood glucose concentration after 1 hour of treatment. (b) Procedures of the therapeutic to study LLC tumor. (c) Time-dependent average tumor growth curves (mean ± SD, n = 5, **p* < 0.05, ***p* < 0.01, and ****p* < 0.001). (d) Resect tumors photograph of LLC tumor-bearing mice with various treatments. (e) Average tumor weights (mean ± SD, n = 5, **p* < 0.05, ***p* < 0.01, and ****p* < 0.001) of LLC tumor-bearing mice after various treatments. (f) Tumor sections with H&E, TUNEL, and Ki-67 staining after various treatments.

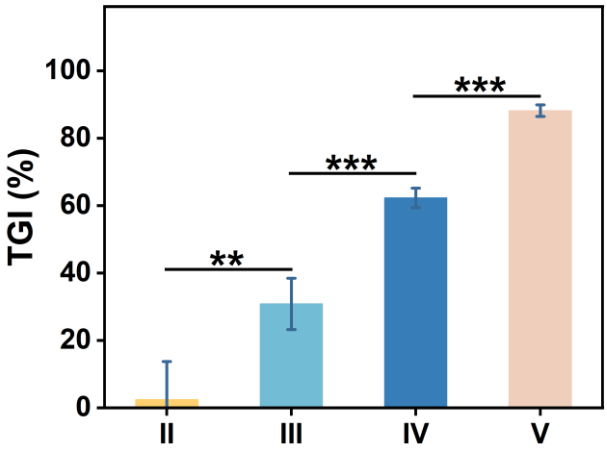

Figure S34. The inhibition rates of subcutaneous tumors in different treatment groups. (II: α-PD-L1; III: FTL; IV: FGTL; II: FGTL + α-PD-L1).

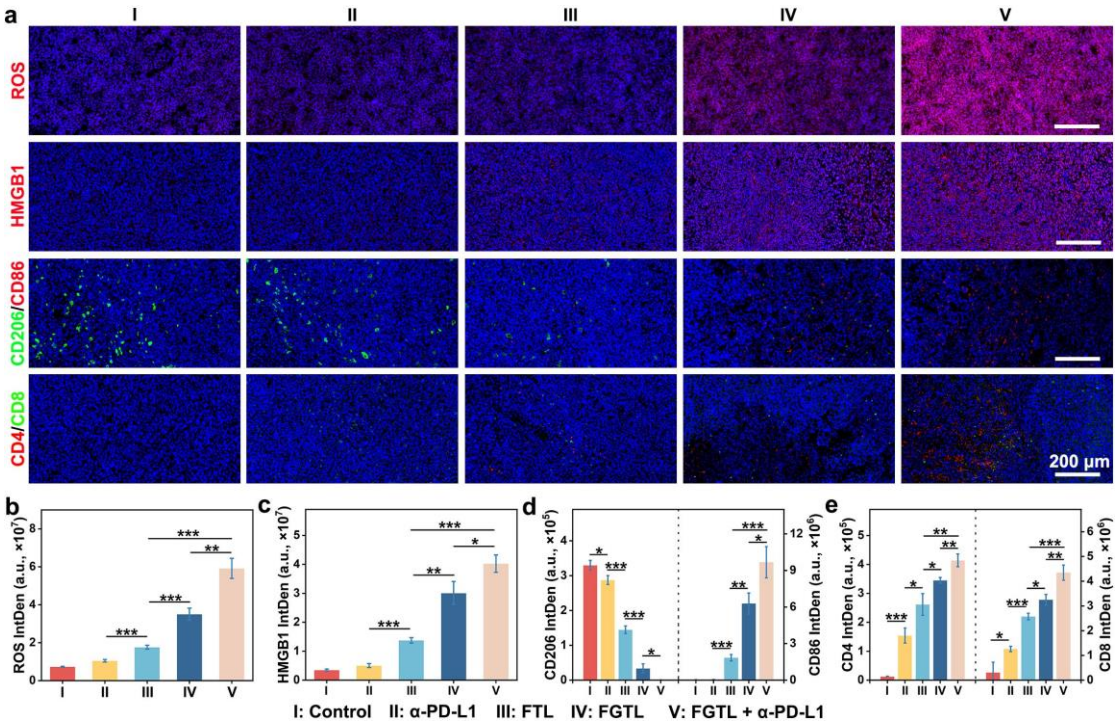

Figure S35. (a) Tumor sections with ROS, HMGB1, CD206/CD86, and CD4/CD8 staining after various treatments and (b-e) the corresponding fluorescence intensity analysis (mean ± SD, n = 3, ***p* < 0.05, ****p* < 0.01, *****p* < 0.001).

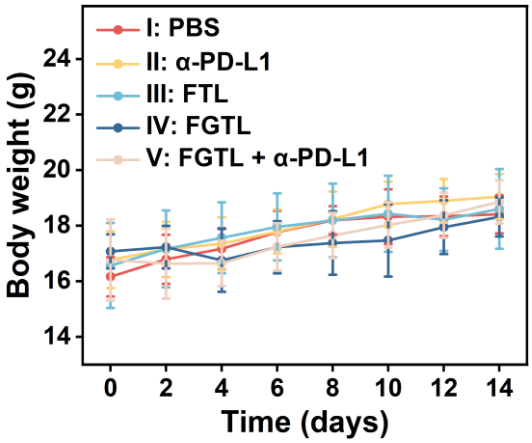

Figure S36. The body weight of subcutaneous LLC tumor-bearing mice after various treatments.

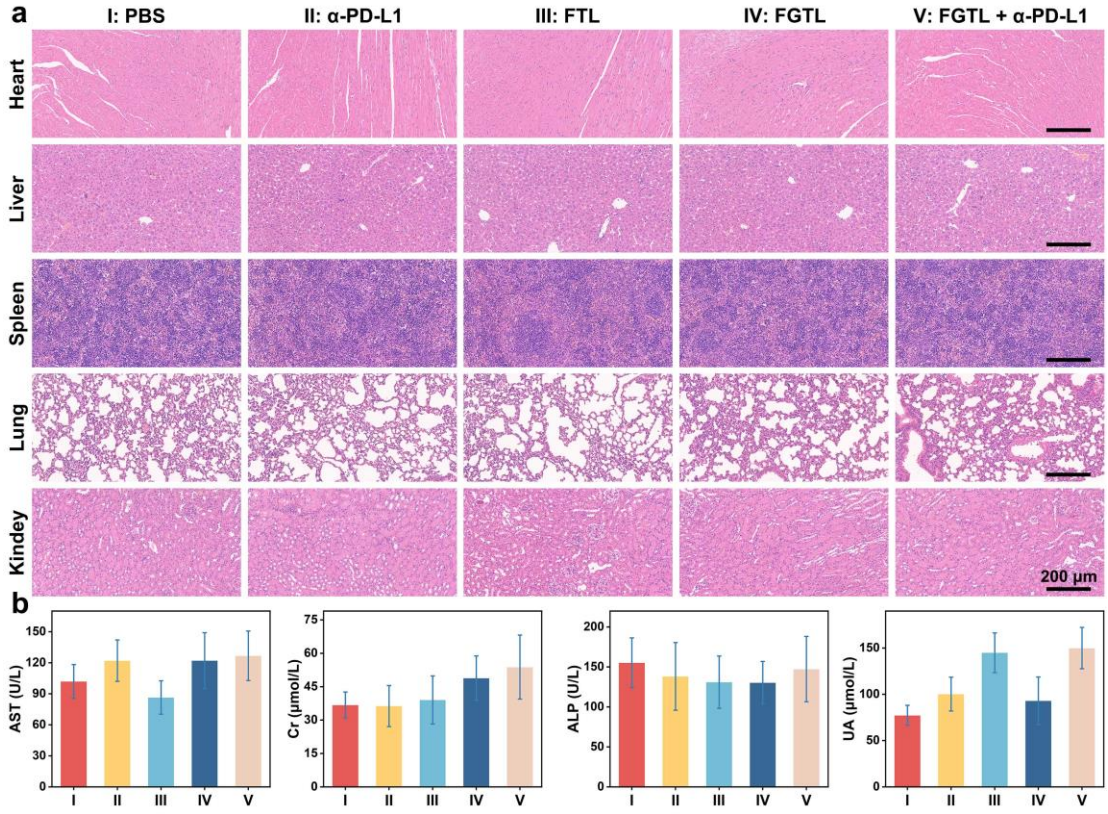

Figure S 37. Biosafety evaluation of mice after various treatments. (a) H&E staining images of organs including the heart, liver, spleen, lung, and kidney obtained from different treatment groups (I: PBS, II: α-PD-L1, III: Fe_3O_4@Tuftsin@Lipids (FTL), IV: FGTL, and V: FGTL plus α-PD-L1). (b) Blood indexes of AST, Cr, ALP, and UA from groups I-V after 14 days of treatment (mean ± SD, n = 5).

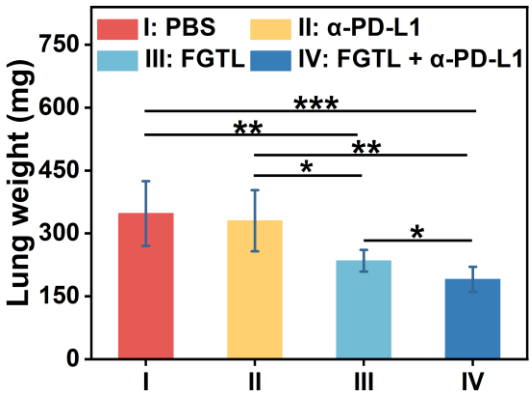

Figure S38. The lung weight of lung metastasis-bearing mice after various treatments (mean ± SD, n = 6, **p* < 0.05, ***p* < 0.01, ****p* < 0.001).

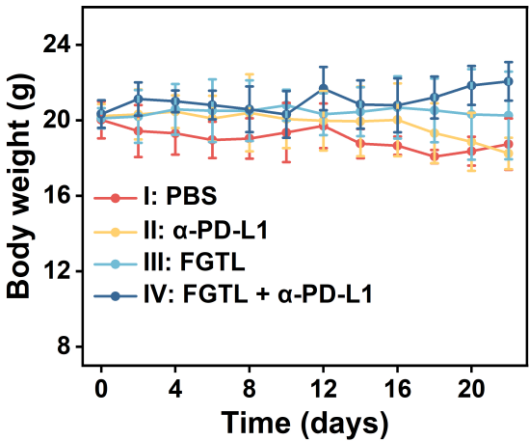

Figure S39. The body weight of lung metastasis-bearing mice after various treatments.

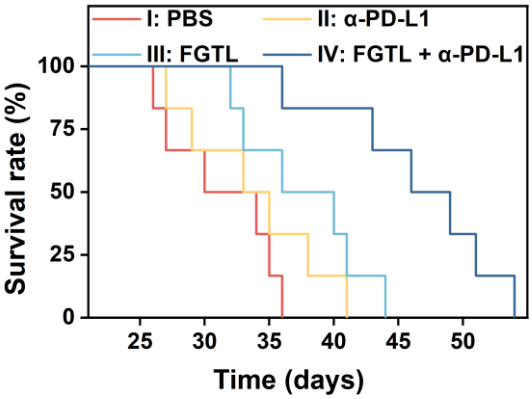

Figure S40. The survival rates of lung metastasis mice after various treatments.

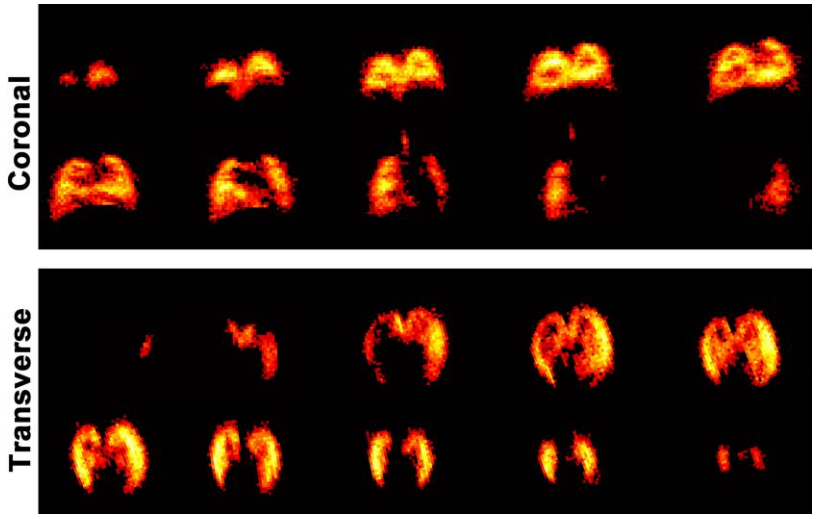

Figure S41. The coronal and transverse ^{129}Xe ventilation MRI of the lung in healthy mice.

References

[1] L. Dai, M. Yao, Z. Fu, X. Li, X. Zheng, S. Meng, Z. Yuan, K. Cai, H. Yang, Y. Zhao, *Nat. Commun.* **2022**, *13*, 2688.

[2] J. Zhu, Y. Zhang, X. Chen, Y. Zhang, K. Zhang, H. Zheng, Y. Wei, H. Zheng, J. Zhu, F. Wu, J. G. Piao, Z. Zhu, F. Li, *Biochem. Biophys. Res. Commun.* **2021**, *534*, 902-907.

[3] a) Z. E. Hu, J. Li, Z. N. Wu, Y. J. Wei, Y. H. Liu, N. Wang, X. Q. Yu, *ACS Biomater Sci Eng* **2021**, *7*, 1394-1402; b) J. Li, Z. E. Hu, Y. J. We, Y. H. Liu, N. Wang, X. Q. Yu, *J Colloid Interface Sci* **2022**, *606*, 1219-1228.

[4] G. Jia, T. Wang, R. Li, X. Li, G. Sun, W. Chen, Y. Peng, C. Cheng, J. Yang, C. Zuo, *Adv Healthc Mater* **2023**, *12*, e2301559.

[5] R. Wang, M. Qiu, L. Zhang, M. Sui, L. Xiao, Q. Yu, C. Ye, S. Chen, X. Zhou, *Adv. Mater.* **2023**, *35*, e2306748.

[6] S. Chen, M. Qiu, R. Wang, L. Zhang, C. Li, C. Ye, X. Zhou, *Bioconjug. Chem.* **2022**, *33*, 1729-1740.

[7] a) M. Zhang, H. Li, H. Li, X. Zhao, Q. Zhou, Q. Rao, Y. Han, Y. Lan, H. Deng, X. Sun, X. Lou, C. Ye, X. Zhou, *Magn. Reson. Med.* **2020**, *84*, 569-578; b) H. Imai, A. Kimura, S. Iguchi, Y. Hori, S. Masuda, H. Fujiwara, *Magn. Reson. Med.* **2010**, *64*, 929-938.